

Inferring the population properties of binary neutron stars with gravitational-wave measurements of spin

Xingjiang Zhu,^{1,2} Eric Thrane,^{1,2} Stefan Osłowski,^{3,2} Yuri Levin,^{4,5,1} and Paul D. Lasky^{1,2}

¹*School of Physics and Astronomy, Monash University, Vic 3800, Australia*

²*OzGrav: The ARC Centre of Excellence for Gravitational Wave Discovery*

³*Centre for Astrophysics and Supercomputing, Swinburne University of Technology, Hawthorn Vic 3122, Australia*

⁴*Physics Department and Columbia Astrophysics Laboratory, Columbia University, New York, NY 10027*

⁵*Center for Computational Astrophysics, Flatiron Institute, New York, NY 10010*

(Dated: May 17, 2022)

The recent LIGO-Virgo detection of gravitational waves from a binary neutron star inspiral event GW170817 and the discovery of its accompanying electromagnetic signals mark a new era for multi-messenger astronomy. In the coming years, advanced gravitational-wave detectors are likely to detect tens to hundreds of similar events. Neutron stars in binaries can possess significant spin, which is imprinted on the gravitational waveform via the effective spin parameter χ_{eff} . We explore the astrophysical inferences made possible by current and future gravitational-wave measurements of χ_{eff} . First—using a fiducial model informed by radio observations—we estimate that $\approx 15 - 40\%$ of binary neutron stars should have spins measurable by advanced detectors ($\chi_{\text{eff}} > 0.01$) assuming the spin axis of the recycled neutron star aligns with the total orbital angular momentum of the binary. Second, using Bayesian inference, we show that it is possible to distinguish between our fiducial model and some extreme initial spin period distributions using $\gtrsim 10$ detections. Third, with $\gtrsim 50$ detections, we can confidently tell whether or not the spin axis of the recycled neutron star tends to be aligned with the binary orbit. Finally, stringent constraints can be placed on neutron star magnetic field decay after $\gtrsim 200$ detections, if the spin periods and magnetic field strengths of Galactic binary neutron stars are representative of the merging population.

I. INTRODUCTION

On August 17, the LIGO [1] and Virgo [2] detectors observed GW170817, the first gravitational-wave (GW) signal from a binary neutron star (BNS) merger [3]. The discoveries of an electromagnetic counterpart, visible across the electromagnetic spectrum, ushered in the highly-anticipated era of multi-messenger astronomy [4, 5]. Improved merger rate estimates now indicate that around 10–200 detections of BNS mergers are expected per year of operation at design sensitivities for Advanced LIGO and Virgo [3, 6]. This will enable detailed studies of the population properties of BNS systems.

In 1974, the first pulsar in a BNS system PSR B1913+16 was discovered in radio pulsar surveys [7, 8]. There are now 15 BNS systems known in our Galaxy [9]. Of particular significance is the Double Pulsar PSR J0737–3039A/B [10, 11]. It remains the only BNS system in which both stars can be observed as radio pulsars. In the standard scenario, the recycled NS in a BNS system gets spun up by accreting matter and angular momentum from its companion [12–16]. The final spin period depends on the rate and duration of the accretion process. There is a tendency for the spin periods of the recycled pulsars to be shorter in closer systems [9]. This can be attributed to the fact that pulsars in wider binaries generally have less time to gain angular momentum before their companion stars detonate as supernovae.

It is generally believed that NSs spin down due to the loss of rotational energy by powering magnetically driven plasma winds [17–19]. Magnetic fields play a key role determining the astrophysical character of a NS (see [20]

and references therein). Understanding the evolution of magnetic fields will give insights into both the physics of NS interiors and the observed population of pulsars in the Galaxy. In this paper, we demonstrate that GW measurements of NS spins may shed new light on NS magnetic field evolution.

The spin of merging compact objects is imprinted on the gravitational waveform. While there are six degrees of freedom describing the two spin vectors, the gravitational waveform depends primarily on a single combination of parameters called the effective spin parameter [21, 22]

$$\chi_{\text{eff}} \equiv \frac{\chi_1 \cos(\theta_1) + q\chi_2 \cos(\theta_2)}{1 + q}. \quad (1)$$

Here, (θ_1, θ_2) are the angles between the spin vectors and the orbital angular momentum vector, $q \equiv m_2/m_1$ is the mass ratio of component masses (m_1, m_2) , and (χ_1, χ_2) are the dimensionless spin magnitudes of the merging objects [23–25],

$$\chi_i = cI_i \omega_i / Gm_i^2. \quad (2)$$

Here $i \in \{1, 2\}$, I is the NS moment of inertia, and ω is the angular spin frequency. Physically, χ_{eff} is the mass weighted sum of the spin projections along the axis of the orbital angular momentum. As χ_{eff} is increased above zero, the merger takes place at a higher frequency, and produces a relatively longer signal in the observing band. Conversely, as χ_{eff} is made increasingly negative, the merger takes place at a lower frequency, producing a relatively shorter signal.

In the case of stellar-mass binary black hole mergers, it has been shown that GW measurements of spin can be used to distinguish different formation channels (see, e.g., [26–29]). Black holes formed through isolated binary evolution are expected to spin in alignment with the binary orbital angular momentum, whereas the spin orientation of black holes in dynamically formed binaries is likely to be isotropically distributed. By combining multiple detections, it is possible to constrain the typical misalignment angle of black hole spins and infer the relative fraction of different sub-populations.

While published GW measurements of GW170817 are consistent with $\chi_{\text{eff}} = 0$ [3], advanced detectors operating at design sensitivity may be able to measure statistically significant spin in BNS inspirals. In this paper, we point out that a significant fraction of future LIGO-Virgo detections may contain measurable signatures of spin. Combining multiple measurements from an ensemble of BNS signals, it will be possible to constrain the *shape* of the χ_{eff} distribution from which we can infer interesting NS population properties. In particular, we show that GW measurements can be used to constrain (1) the typical misalignment angle between the NS spin axis and the orbital angular momentum and (2) the decay timescale of NS magnetic fields.

The organization of this paper is as follows. In Section II, we present a fiducial model of NS spin distribution that we use to investigate how GWs might inform our understanding of NS evolution. The model is built to be consistent with radio observations, but it does not necessarily cover the full range of possible scenarios. Additional details are provided in Appendices A and B. In Section III, we discuss the sensitivity of advanced detectors to measure NS spins. In Section IV, we present a Bayesian framework for inference of BNS population properties. We demonstrate model selection and hyper-parameter estimation using Monte-Carlo data. Finally, in Section V, we provide concluding remarks.

II. FIDUCIAL MODELS

In order to link GW measurements to NS evolution, we need to know $\pi(\chi_{\text{eff}}|M, \vec{\Lambda})$: the probability density function for the effective spin parameter χ_{eff} at merger given a model M with population hyper-parameters $\vec{\Lambda}$. The idea is that by measuring χ_{eff} , we can make inferences about the NS evolutionary properties described by the hyper-parameters $\vec{\Lambda}$. For example, we investigate our ability to constrain the NS magnetic field decay timescale $\tau_B \in \vec{\Lambda}$. Here we present a suite of fiducial models that represent plausible distributions of $\pi(\chi_{\text{eff}}|M, \vec{\Lambda})$ for illustrative purposes.

We construct four fiducial models, labeled as STANDARD, ISO SPIN, B DECAY, and DIFF EOS. Each model corresponds to a different vector of hyper-parameters $\vec{\Lambda}$. We provide an overview of the fiducial models for

$\pi(\chi_{\text{eff}}|M, \vec{\Lambda})$. More details on the construction of these models are given in Appendices A and B.

To construct each fiducial model, we first construct the probability density function $\pi(\vec{\lambda}_0)$ for a vector of parameters $\vec{\lambda}_0$ describing the BNS system at the time of its birth. These parameters include: component masses, spin periods, magnetic field strengths, binary orbital period and eccentricity. This eight-dimensional distribution is constructed using observations of known Galactic BNS systems. Next, we evolve the at-birth parameters $\vec{\lambda}_0$ forward in time in order to obtain a new distribution $\pi(\vec{\lambda}_m)$, which describes these same parameters at the time of merger. In order to carry out this calculation, we assume that NSs spin down due to magnetic dipole braking [30] and the spin tilt angles do not evolve over time. We follow the NS spin evolution and binary orbital evolution from the birth of the second NS to the binary merger. Finally, we calculate χ_{eff} using the at-merger spin periods. We treat the typical tilt angle of NS spin vectors, the equation of state and the magnetic field decay timescale as hyper-parameters included in $\vec{\Lambda}$.

It is useful to note that the vector of hyper-parameters $\vec{\Lambda}$ describes the *population* of BNSs. This may be contrasted with parameters $(\vec{\lambda}_0, \vec{\lambda}_m)$, which describe the properties of an individual binary (at birth and at merger respectively). The equation of state is an example of a hyper-parameter since it is a property of the population as a whole. The NS masses are an example of a parameter since they are different for each BNS.

Our STANDARD model assumes that the spin axis of the recycled NS is aligned with the total binary orbital angular momentum. That is, $\cos\theta_1 = 1$. This is a plausible assumption given that the only measured misalignment angle (which comes from the Double Pulsar) is small: $< 3.2^\circ$ at 95% confidence, assuming that the observed emission comes from both magnetic poles which is the scenario favored by radio data [31]. We assume that the magnetic field decay time is long compared to the age of the Universe. We assume the AP4 equation of state [32].

The ISO SPIN model is identical to the STANDARD model except we assume that $\cos\theta_1$ is drawn from a uniform distribution. While this model is disfavored by the Double Pulsar, we include it in order to demonstrate how GW measurements can help distinguish between STANDARD and ISO SPIN.

The B DECAY model is identical to STANDARD, except that we assume an exponentially decaying magnetic field [33] with a decay timescale $\tau_B = 170$ Myr [20].

The DIFF EOS model is identical to STANDARD, except that we use the PAL1 equation of state instead of AP4 (see [32] and references therein). For a mass of $1.4 M_\odot$, the NS radius is ≈ 14 km for PAL1 compared to ≈ 11 km for AP4. Therefore, larger values of χ_{eff} are predicted for PAL1 compared to the AP4 equation of state all else equal.

In addition to the four fiducial models, we also consider a population synthesis model from [34] denoted

Model	θ_1	B-field decay	EOS	note
STANDARD	aligned	no	AP4	Empirical
ISO SPIN	isotropic	no	AP4	Empirical
B DECAY	aligned	170 Myr	AP4	Empirical
DIFF EOS	aligned	no	PAL1	Empirical
POPSYNTH1	aligned	yes	AP4	Pop. Synth.

TABLE I. Summary of BNS population models considered in this work. Empirical models are developed based on radio pulsar observations of 15 Galactic BNS systems. For details, see Section II and Appendices A and B. Model POPSYNTH1 is a population synthesis model from [34].

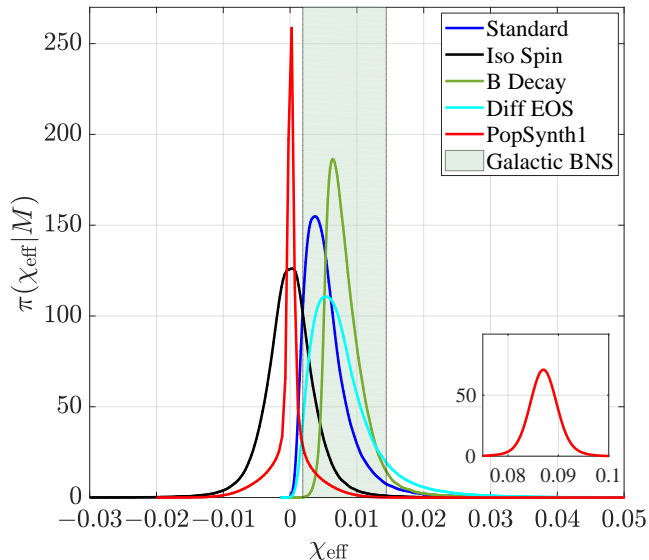


FIG. 1. Probability density distribution of χ_{eff} expected for a population of BNS inspiral events for 5 different models (Table I). The secondary peak of POPSYNTH1 is shown as an inset for better comparison of the features among different models. The vertical shaded region indicates a likely range expected for Galactic BNS systems at merger (Table II).

here as POPSYNTH1. In this model, if a common envelope phase occurs before the formation of the second NS, there is an episode of hyper-critical accretion. This allows a large amount of matter to be accreted compared to other models in [34]. In this model, the magnetic field decays until reaching a minimum of 10^8 G. As a consequence, roughly half of the recycled NSs are spun up during a subsequent Roche-lobe overflow phase to spin periods of ≈ 3 ms, while the rest spin at a much slower rate; see the model HP in Fig. 3 in Ref. [34].

The five models are summarized in Table I. The corresponding distributions $\pi(\chi_{\text{eff}}|M)$ are shown in Fig. 1. Each colored curve corresponds to a different model. For reference, we also plot as a shaded vertical band the range of χ_{eff} expected at merger for the 7 Galactic BNS systems that consist of a recycled pulsar and that will merge within a Hubble time. We evolve the spin periods forward until the merger, which will happen in between

Pulsar in BNS systems	$\chi_{\text{eff}}^{\text{low}}$ ($\times 10^{-3}$)	$\chi_{\text{eff}}^{\text{high}}$ ($\times 10^{-3}$)	\mathcal{R} (Gyr^{-1})	Chirp mass (M_{\odot})
J1757–1854	10.0	14.4	4.84	1.189
J0737–3039A/B	9.5	14.0	7.39	1.125
J1913+1102	8.3	12.1	0.32	1.243
B2127+11C	4.5	8.3	3.19	1.181
J1756–2251	4.2	11.6	0.48	1.118
B1913+16	2.1	4.3	2.44	1.231
B1543+12	1.9	7.9	0.34	1.166

TABLE II. Effective spins for 7 Galactic BNS systems at the time of merger (see text for details).

76 Myr and 2.7 Gyr. We consider two cases. We calculate $\chi_{\text{eff}}^{\text{low}}$ assuming no magnetic field decay and using the AP4 equation of state. We calculate $\chi_{\text{eff}}^{\text{high}}$ assuming the PAL1 equation of state and magnetic field decay with a timescale of 170 Myr. The results are listed in Table II. Also included are the chirp mass and the relative merger rate \mathcal{R} defined as the reciprocal of the sum of pulsar characteristic age and binary coalescence time. We use the B pulsar’s age when calculating \mathcal{R} for the Double Pulsar. Details of the calculation and information about all known Galactic BNS systems are given in Appendices A and B. We assume the other systems are similar to the Double Pulsar, i.e., the spin axis of the recycled pulsar is aligned with the binary orbit and the companion NS has effectively zero spin. Out of 7 binaries, at least 2 are expected to have $\chi_{\text{eff}} \gtrsim 0.01$.

There are a number of interesting features worthy of remark in Fig. 1. First, for all five models, a significant fraction of BNS (15-50%) are characterized by relatively large spins with $\chi_{\text{eff}} > 0.01$. We note that, for our four fiducial models, essentially all of the events possess $|\chi_{\text{eff}}| < 0.05$, consistent with the “low-spin” prior used in the GW170817 discovery paper [3].

Second, we see that POPSYNTH1 predicts a dramatically different distribution. While half of the population has $|\chi_{\text{eff}}| < 0.01$, the other half possess much larger spins with $\chi_{\text{eff}} \in (0.08, 0.1)$. We note that such high spins are not supported by current radio observations for pulsars with NS or massive white dwarf companions. We show that it is possible to definitively test POPSYNTH1 with a small number of detections in section IV A.

Third, there are clear differences between different fiducial models. In the STANDARD model, χ_{eff} is found to be between 0 and 0.03 with $\gtrsim 99\%$ probability. In the ISO SPIN model, the distribution is symmetric with respect to zero spin and $|\chi_{\text{eff}}| \lesssim 0.02$. B DECAY and DIFF EOS predict higher values of χ_{eff} than STANDARD, extending the high end to 0.04. For DIFF EOS, this is because of larger NS radii allowed by PAL1 than the AP4 equation of state. For B DECAY, this is because of lower spin-down rates. The peak position of B DECAY depends on the magnetic field decay timescale, which can be constrained using a large number of BNS detections given our prior knowledge of the equation of state. We demonstrate this in Section IV B.

III. MEASUREMENT UNCERTAINTY OF SPIN USING ADVANCED DETECTORS

In order to compare the distributions of χ_{eff} to the sensitivity of advanced detectors, we carry out Monte-Carlo simulations. We inject a series of BNS signals into Gaussian noise generated assuming Advanced LIGO design sensitivity [35]. We obtain the marginalized posterior distribution for χ_{eff} using the parameter estimation code LALINFERENCE [36]. We employ the low-spin prior, i.e., $|\chi_{\text{eff}}| < 0.05$ with a flat distribution in $(-0.05, 0.05)$ for both component spins, as used for GW170817. We use the phenomenological inspiral-merger-ringdown (IMR-PHENOMP) waveform model [37] and set the low frequency cutoff at 30 Hz. The IMR-PHENOMP model allows us to employ reduced order modeling and reduced order quadrature, which significantly speeds up calculations [38]. The model does not include tidal effects, whereas a real search must simultaneously account for the effects of spins and tides. We note that the contribution to GW phase evolution from tidal effects is decoupled from that of spins to the level of numerical relativity uncertainties (see, e.g., [39]) and thus tidal effects and spins are only weakly correlated through their correlations with mass ratio. A detailed investigation on this issue is beyond the scope of this paper and we focus on the approximate sensitivity of GW detectors to NS spins.

We simulate nine events equally spaced between 80 Mpc and 240 Mpc. The masses are set to $(m_1, m_2) = (1.338, 1.249) M_{\odot}$, matching the Double Pulsar. The right ascension ($13^{\text{h}} 10^{\text{m}}$), declination ($-23^{\circ} 23'$), and GPS time (1187008882) are chosen to match GW170817. The effective spin parameter is set to $\chi_{\text{eff}} = 0.025$, which is at the high end of the distribution in our fiducial models. The inclination angle ι , the polarization angle ψ , and the phase at coalescence ϕ_c are all set to zero. Our choice of source parameters is somewhat arbitrary, but the purpose of the LALINFERENCE runs is to obtain the approximate scaling law between the realistic measurement uncertainty of χ_{eff} and the signal-to-noise ratio (S/N). The exact choice of source parameters does not significantly impact this scaling law.

An example posterior distribution of χ_{eff} produced using LALINFERENCE is provided in Fig. 2. This event is simulated at a distance of 200 Mpc. The expected S/N for a LIGO Hanford-Livingston detector network is 17.4. The posterior samples are well fit by a Gaussian distribution with mean 0.021 and standard deviation, $\sigma_{\chi} = 0.007$ (blue curve). In general, we find that the marginalized posterior distribution of χ_{eff} from LALINFERENCE runs on simulated data can be well approximated by a Gaussian distribution.

In Fig. 3, we plot σ_{χ} as a function of S/N , which is well approximated by the $\sigma_{\chi} \propto (S/N)^{-1}$ scaling law [40]. Using this relation, we can speed up subsequent simulations by approximating the reduced likelihood function

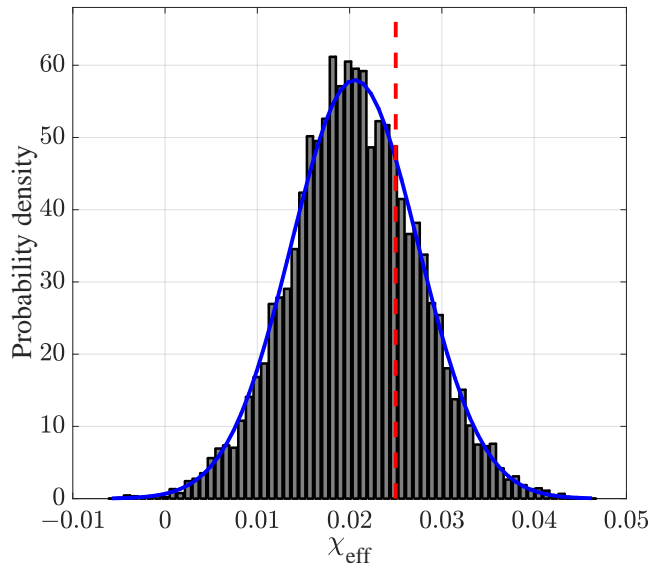


FIG. 2. A posterior distribution for χ_{eff} generated with Monte Carlo data. The data consist of a BNS signal at 200 Mpc added to Hanford and Livingston design sensitivity noise. The blue curve is the Gaussian distribution with the mean value and standard deviation determined from posterior samples. The red vertical line marks the true injection value.

as a Gaussian distribution with width σ_{χ}

$$\mathcal{L}(h|\chi_{\text{eff}}) \propto N(\chi_{\text{eff}}^{\text{ML}}, \sigma_{\chi}), \quad (3)$$

where the mean $\chi_{\text{eff}}^{\text{ML}}$ is the maximum-likelihood estimate for a particular random noise realization. Each value of $\chi_{\text{eff}}^{\text{ML}}$ is generated by adding a normally-distributed random number (variance = σ_{χ}^2) to the true value of χ_{eff} .

We simulate 10^4 BNS sources that are uniformly distributed in volume (i.e., uniform in distance cubed) out to 300 Mpc. Note that within such a distance we can safely ignore the merger rate evolution over redshift. The other source parameters such as sky location and inclination angle are appropriately randomized according to suitable distributions.

We calculate the (expectation value of) S/N for the Advanced LIGO Hanford-Livingston detector pair. Events with a network matched-filter $S/N < 12$ are excluded because they fall below the threshold necessary for unambiguous detection [41]. This leads to about 2000 detected events. As expected, the distribution of S/N is consistent with $p(S/N) \sim (S/N)^{-4}$ [42]. The median S/N in our Monte Carlo dataset is 15, which corresponds to an effective spin measurement uncertainty of $\sigma_{\chi} \approx 0.008$ (see Fig. 3).

For comparison, we also show the GW170817 uncertainty for the low-spin prior as a black square in Fig. 3. The numerical value $\sigma_{\chi} \approx 0.009$ is computed by approximating the published 90% confidence ($\approx 1.6\sigma$) interval $(-0.01, 0.02)$ [3] with a Gaussian distribution. At the same S/N , the measurement sensitivity of χ_{eff} given by

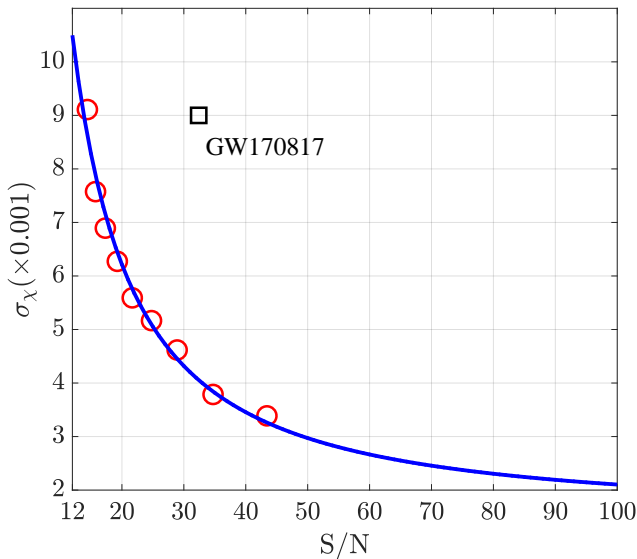


FIG. 3. The standard deviation (σ_χ) of posterior distribution of χ_{eff} as a function of signal to noise ratio (S/N). Red circles are measured by running parameter estimation code LALINFERENCE on Monte-Carlo data at Advanced LIGO design sensitivity. The blue curve is the $\sigma_\chi \propto (S/N)^{-1}$ approximation used in simulations. We only consider $S/N > 12$ as required for an unambiguous detection. The black square is for GW170817 with $S/N = 32.4$ and $\sigma_\chi = 0.009$.

our scaling law (depicted by the blue curve in Fig. 3) is a factor of 2 better than that of GW170817. This may be due to the combined effects of 1) better sensitivity at low frequency, which is critical to measure the GW phase evolution and thus spin effects, 2) systematic errors of waveform models and 3) calibration uncertainties of real data. Specifically, for the analysis of GW170817 [3], i) a different waveform model was used to account for both tidal effects and spins, which leads to different statistical uncertainties for χ_{eff} and ii) the subtraction of the glitch that was superposed on the signal in the LIGO-Livingston data could have impacted the uncertainties for parameter estimates. Furthermore, our scaling law for σ_χ is derived using simulations with a single mass ratio ($q = 0.93$), whereas for GW170817 there is significant support for smaller values of q . Since 90% of our simulated BNSs have $0.8 \leq q \leq 1$ [43] given the mass distributions derived in Section B, we believe our conclusions are only slightly affected by our choice of q .

We compare Advanced LIGO’s sensitivity to measure χ_{eff} with the effective spins of Galactic BNS systems at the time of merger (Table II). In Fig. 4, we show the luminosity distance out to which χ_{eff} can be measurable at the $2\text{-}\sigma$ level. Blue open circles are Galactic BNS systems, taking the lower values of χ_{eff} listed in Table II. We assume an optimal binary orientation ($\cos \iota = 1$) and all systems are placed at the sky location of GW170817. The size of the blue circles are proportional to the relative merger rate \mathcal{R} (see Table II) of the particular sys-

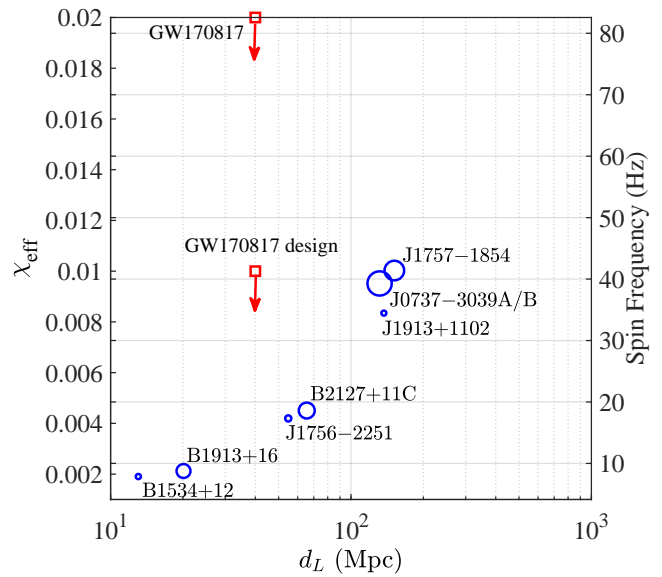


FIG. 4. A schematic diagram showing the sensitivity of Advanced LIGO to measure χ_{eff} . d_L is the approximate luminosity distance out to which χ_{eff} is measurable at the $2\text{-}\sigma$ level assuming optimal binary orientation. Galactic BNS systems (blue circles) are placed at the sky location of GW170817. Also shown is the published upper limit and the expected limit at design sensitivity for GW170817. A second y-axis shows the spin frequency of the recycled NS.

tem. Red squares with downwards arrows indicate the upper limit for GW170817 and the expected limit at design sensitivity. Note that the GW170817 design limit lies above the linear trend of blue circles; the distance is about 0.005, which can be attributed to the asymmetric 90% confidence interval $(-0.01, 0.02)$ [3].

To put Fig. 4 into an astrophysical context, we add a second y-axis for the spin frequency of the recycled NS in Fig. 4. The conversion from χ_{eff} to the spin frequency employs the average mass of 7 recycled pulsars and $\chi_{\text{eff}} = \chi_1/2$, i.e., assuming $\chi_2 = 0$ and $q = 1$; see Eqs. (1-2). We show that Advanced LIGO operating at design sensitivity will be sensitive to $\chi_{\text{eff}} \sim 0.01$ up to ~ 140 Mpc. Out of 7 known Galactic BNS systems, 2 ($\sim 30\%$) are above this threshold assuming aligned spin. Given the relatively higher merger rate for these two systems, an even larger fraction of merging BNS should have measurable spins.

IV. BAYESIAN INFERENCE

In this section, we present a Bayesian formalism to infer BNS population properties from GW measurements of χ_{eff} . In subsection IV A, we demonstrate how GW measurements from an ensemble of detections can be used to carry out model selection, thereby allowing us to differentiate between the different models in Table I. In subsection IV B, we show how to constrain the magnetic field decay timescale using a large number of detections.

A. Model selection

Let $\mathcal{L}(h|\vec{\theta})$ be the likelihood of GW data h given BNS parameters $\vec{\theta}$. The GW parameter space includes 15 or more parameters including, e.g., inclination angle, luminosity distance, and component masses. Here, however, we are only concerned with χ_{eff} . Thus, we marginalize over every parameter except χ_{eff} to obtain a marginalized likelihood function $\mathcal{L}(h|\chi_{\text{eff}})$.

The Bayesian evidence for a model M given the data h is

$$\mathcal{Z}(h|M) = \int d\chi_{\text{eff}} \mathcal{L}(h|\chi_{\text{eff}}) \pi(\chi_{\text{eff}}|M), \quad (4)$$

where $\pi(\chi_{\text{eff}}|M)$ is the conditional prior distribution for χ_{eff} given a model $M \in \{\text{STANDARD}, \text{ISO SPIN}, \text{DIFF EOS}, \text{POPSYNTH1}, \text{B DECAY}\}$. Rewriting Eq. 4 in terms of posterior samples [44], we obtain

$$\mathcal{Z}(h|M) = \sum_{i=1}^{n_k} \frac{\pi(\chi_{\text{eff}}^i|M)}{\pi(\chi_{\text{eff}}^i|\text{LAL})}. \quad (5)$$

Here, the index i runs over n_k posterior samples, each corresponding to a different value of χ_{eff} ; see also Eq. (7) in [28]. $\pi(\chi_{\text{eff}}|\text{LAL})$ is the prior used by LALINFERENCE in order to obtain the initial set of posterior samples. It appears in Eq. 5 in order to convert the posterior distribution output by LALINFERENCE into a likelihood. Since Model POPSYNTH1 predicts a significant fraction of BNS events with $\chi_{\text{eff}} > 0.05$, $\pi(\chi_{\text{eff}}|\text{LAL})$ is set as $\chi_{\text{eff}} < 0.1$ with a flat distribution for both χ_1 and χ_2 in $(-0.1, 0.1)$ throughout this work. This is wider than the low-spin prior used for actual LALINFERENCE simulations. This makes our results slightly optimistic by less than a factor of 2. We simulate 10^4 mock posterior samples using the Gaussian likelihood function defined in Eq. (3).

The total evidence from N detections is simply the product of the evidence for each detection:

$$\mathcal{Z}_{\text{tot}}(\{h\}|M) = \prod_{k=1}^N \mathcal{Z}(h_k|M). \quad (6)$$

The Bayes factor (BF) comparing model M_1 and model M_2 is given by

$$\text{BF}_{1,2} = \frac{\mathcal{Z}_{\text{tot}}(h|M_1)}{\mathcal{Z}_{\text{tot}}(h|M_2)}. \quad (7)$$

Following convention [44], we impose a threshold of $\ln(\text{BF}) = 8$ ($\sim 3.6\sigma$) to define the point beyond which one model is significantly favored over another.

In order to demonstrate model selection, we carry out a Monte Carlo simulation as described in Section III. We use the scaling relation between σ_χ and S/N shown in Fig. 3 and the Gaussian likelihood function $\mathcal{L}(h|\chi_{\text{eff}})$ in Eq. 3. The calculation assumes a two-detector Advanced LIGO network operating at design sensitivity.

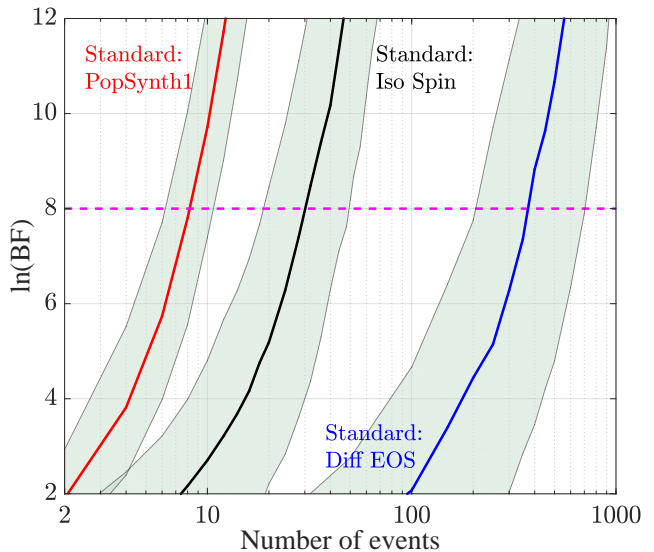


FIG. 5. Bayes Factor (BF) as a function of the number of events between models STANDARD (the true underlying model), ISO SPIN, DIFF EOS and POPSYNTH1. The shaded regions correspond to $1\text{-}\sigma$ confidence intervals.

Then, we calculate three different Bayes factors (plotted in Fig. 5 as a function of the number of events): STANDARD / ISO SPIN (black), STANDARD / POPSYNTH1 (red) and STANDARD / DIFF EOS (blue). The colored lines show the median value while the shaded region indicates the $1\text{-}\sigma$ confidence interval.

When $\ln \text{BF}_{1,2} \gtrsim 8$, we are able to clearly distinguish between the STANDARD model and the three alternatives considered here. The red curve shows that advanced detectors can distinguish between STANDARD and the (extreme) $\pi(\chi_{\text{eff}})$ distribution of POPSYNTH1 after only ≈ 11 detections. The black curve shows that advanced detectors can distinguish between STANDARD and ISO SPIN after ≈ 50 events. Finally, the blue curve shows that advanced detectors can distinguish between STANDARD and DIFF EOS after ≈ 700 events.

B. Constraining magnetic field decay

Given a NS equation of state, one can construct a posterior for magnetic field decay timescale τ_B

$$p(\tau_B|h, M) \propto \pi(\tau_B) \int d\chi_{\text{eff}} \mathcal{L}(h|\chi_{\text{eff}}) \pi(\chi_{\text{eff}}|M, \tau_B) \quad (8)$$

Here $\pi(\tau_B)$ is the prior distribution for τ_B , which is assumed to be log-uniform on the interval (1 Myr, 10^4 Myr). Note that such a wide prior is used only as an example to test our method and does not fold in any theoretical or observational information. Our primary purpose here is to demonstrate how many

GW detections are required to place stringent constraints on τ_B using GW data alone. The distribution $\pi(\chi_{\text{eff}}|M, \tau_B)$ is the conditional prior for χ_{eff} given model M and the decay timescale τ_B . An example conditional prior is represented visually in Fig. 1 for Model B DECAY with $\tau_B = 170$ Myr.

Marginalizing over χ_{eff} , we obtain a posterior on τ_B . In practice, we do not carry out an integral over a continuous variable; we sum up posterior samples. The discrete version for Eq. (8) is

$$p(\tau_B|h, M) \propto \pi(\tau_B) \sum_{i=1}^n \frac{\pi(\chi_{\text{eff}}^i|M, \tau_B)}{\pi(\chi_{\text{eff}}^i|\text{LAL})}. \quad (9)$$

Generalizing to N events, the posterior for τ_B becomes

$$p(\tau_B|h, M) \propto \pi(\tau_B) \prod_{k=1}^N \sum_{i=1}^{n_k} \frac{\pi(\chi_{\text{eff}}^{i,k}|M, \tau_B)}{\pi(\chi_{\text{eff}}^{i,k}|\text{LAL})}. \quad (10)$$

Here, $\chi_{\text{eff}}^{i,k}$ represents the i^{th} posterior sample from the k^{th} event.

Following the same procedure described in Subsection IV A, we generate an ensemble of detections. Events are generated using the B DECAY model with the true value of $\tau_B = 170$ Myr. In order to infer τ_B using Eq. (10), we generate $\pi(\chi_{\text{eff}}|M, \tau_B)$ for a vector of τ_B equally spaced in log space between 1 Myr and 10 Gyr.

Fig. 6 shows the posterior distribution $p(\tau_B|h, M)$ inferred from 200 events. The true magnetic field decay timescale $\tau_B = 170$ Myr is marked with a red vertical line. We repeat the simulation for 100 times to account for random noise fluctuations. The typical 1- σ variations are shown as the shaded region in Fig. 6. For $\sim 95\%$ of noise realizations, the true value of τ_B is recovered within the 2- σ confidence interval. In this example, we find that τ_B can be constrained to be between 10 Myr and 1 Gyr with $\gtrsim 90\%$ confidence with 200 detections.

V. DISCUSSION AND CONCLUSIONS

The detection of the BNS inspiral event GW170817 has opened up new opportunities to study NS physics. In the next five years, observations of similar events will become increasingly more frequent as Advanced LIGO/Virgo approach their design sensitivities and new detectors such as KAGRA [45] and LIGO-India [46] start to operate. As advanced detectors observe tens, and eventually hundreds, of BNS inspirals, it will be possible to make inferences about NS population properties using GW observations. We demonstrate that GW measurements of spin will have implications for the minimum NS spin period for BNSs after ~ 10 events, for the typical spin tilt angle of NSs after tens of detections, and for the NS magnetic field evolution after hundreds of observations.

In this proof-of-concept analysis, we rely on a set of fiducial models. The models are constructed to be consistent with radio pulsar observations, but they do not

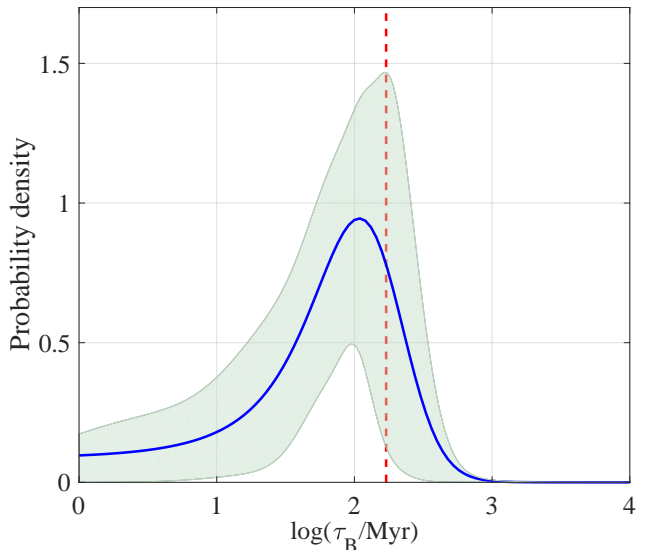


FIG. 6. The mean posterior distribution (blue curve) and its typical variation (shaded region) of the magnetic field decay timescale τ_B recovered using 200 events. The red vertical line marks the true injection value.

necessarily represent the full range of allowable parameter space. While the fiducial models are suitable for illustrative purposes, the next step in this program is to develop a more nuanced model, which *does* allow for the full range of possible initial conditions. It should be possible to then combine all available radio and GW data within a single Bayesian framework, yielding optimal constraints on NS evolution.

Our fiducial model does not account for selection effects associated with detecting radio pulsars in BNS systems. We assume that Galactic BNSs detected in radio are representative of merging binaries detectable with GWs. That is, pulsar luminosities are independent of their spin periods and magnetic field strengths. In practice, even though such an assumption holds, pulsars with shorter spin periods are more difficult to find in radio surveys. In future studies, it will be necessary to carefully include all selection effects in a formulation that attempts to combine GW and radio data.

We find that 2 out of 7 ($\sim 30\%$) of the known BNS systems that will merge within a Hubble time have spins that are marginally detectable up to 140 Mpc by Advanced LIGO operating at design sensitivity. The true fraction of BNSs with measurable spins may be higher since short-lived binaries like those two systems are less likely to be observed in radio. Our standard fiducial model assumes the spin axis is aligned with the binary orbital angular momentum and we do not consider spin precession effects. While this is a second-order effect, more information can be extracted by searching for precessing binaries.

In this work, we focus on BNS systems formed via the isolated binary evolution channel. It is generally be-

lieved that there is insufficient time for the recycled NS to reach ms spin periods and the second NS spins down much faster and thus makes no contribution to the effective spin at the time of binary merger. While our fiducial models predict that essentially all merging BNS have $|\chi_{\text{eff}}| < 0.05$, binaries formed via dynamical captures could have much larger spins. Measurements of NS spins outside our fiducial model prediction will have interesting implications about their formation history.

Finally, our analysis does not account for NS tidal effects. Although there is not strong covariance between χ_{eff} and NS tidal parameters, simultaneously fitting for both spins and tides would result in different statistical errors for χ_{eff} measurements. Comparing our assumed sensitivity with spin constraints for GW170817 indicates that our results might be overly optimistic, but by no more than a factor of two. Additionally, we find there is a degeneracy between NS equation of state and magnetic field evolution for the χ_{eff} distribution of BNS mergers. Constraints on NS magnetic field decay using the analysis method proposed in this paper would rely on prior knowledge on the equation of state. After tens to hundreds of BNS detections, measurements of NS tidal effects and possibly post-merger signatures will place tight constraints on the equation of state and thus allow us to study NS magnetic field evolution with spin [47].

ACKNOWLEDGMENTS

We thank Matthews Bailes, Salvatore Vitale, Simon Stevenson and Christopher Berry for helpful comments on the manuscript and Colm Talbot, Rory Smith, Alexander Heger, Bernhard Müller, Sylvia Biscoveanu, Lijing Shao, Shuxu Yi and Gang Wang for useful discussions. XZ, ET & YL are supported by ARC CE170100004. ET is supported through ARC FT150100281. SO acknowledges support through the ARC Laureate Fellowship grant FL150100148. PDL is supported through ARC FT160100112 and ARC DP180103155. This is LIGO Document LIGO-P1700400.

Appendix A: NS spin evolution and BNS inspirals

Here we describe the calculations necessary to evolve the at-birth parameters $\vec{\lambda}_0$ of BNS systems to the parameters at merger $\vec{\lambda}_m$ as outlined in Section II. We construct the distribution of these parameters, such as NS mass, spin and binary orbital period and eccentricity, using radio pulsar observations in section B.

The coalescence time of a circular binary due to the emission of GWs is [48]

$$T_{c,\text{circ}} = \frac{5c^5}{256(2\pi f_0)^{8/3}(GM_c)^{5/3}}, \quad (\text{A1})$$

where f_0 is the initial binary orbital frequency, M_c is the chirp mass defined as $M_c = M\eta^{3/5}$, with $M = m_1 + m_2$

being the total mass, and $\eta = m_1 m_2 / M^2$ is the symmetric mass ratio. The coalescence time for an eccentric binary can be computed as [49, 50]

$$T_c = \frac{15c^5}{304} (2\pi f_0)^{-8/3} (GM_c)^{-5/3} a_0^4 \int_0^{e_0} g(e) de. \quad (\text{A2})$$

Here e_0 is the initial binary orbital eccentricity, the constant a_0 and the function $g(e)$ are

$$a_0 = (1 - e_0^2) e_0^{-12/19} \left(1 + \frac{121}{304} e_0^2 \right)^{-870/2299}, \quad (\text{A3})$$

$$g(e) = e^{29/19} (1 - e^2)^{-3/2} \left(1 + \frac{121}{304} e^2 \right)^{1181/2299}. \quad (\text{A4})$$

For an eccentric binary, the orbital frequency and eccentricity co-evolve as

$$\frac{f(e)}{f(e_0)} = \left[\frac{\sigma(e_0)}{\sigma(e)} \right]^{3/2}, \quad (\text{A5})$$

where the function $\sigma(e)$ is defined as

$$\sigma(e) = \frac{e^{12/19}}{1 - e^2} \left(1 + \frac{121}{304} e^2 \right)^{870/2299}. \quad (\text{A6})$$

Evolving the BNS systems listed in Table III that will merge within a Hubble time forward in time, we find that they are expected to be in nearly circular orbits ($e \lesssim 10^{-6}$) when they enter the sensitive frequency band ($f > 10$ Hz) of ground-based interferometers in between 76 Myr and 2.7 Gyr.

Assuming magnetic dipole braking, the NS spin frequency evolution follows [51]:

$$\dot{\omega} = -K\omega^3, \quad (\text{A7})$$

where $\omega = 2\pi/P$ with P being spin period, $\dot{\omega} = d\omega/dt$. The torque parameter K is defined as [19]

$$K = \frac{B^2 R^6}{c^3 I} (1 + \sin^2 \alpha), \quad (\text{A8})$$

where B is the surface magnetic field strength, R is the NS radius, I is the moment of inertia, α is the misalignment angle between the magnetic dipole moment and spin axis. There are a few notes worthy of mentioning here. First, Eq. A8 is a convenient approximation to numerical results found in [19]. Second, there is a degeneracy between B and α . Since pulsar measurements collected here only allow us to infer K , we choose to fix α at 30° . The exact value of α is not important as the overall spin-down behavior is determined by K . Third, the spin-down estimator of B can be derived from $P\dot{P} = 4\pi^2 K$ where P and \dot{P} is the spin period and period derivative respectively.

The moment of inertial I can be computed as

$$I \simeq 0.237mR^2 \left[1 + 4.2 \frac{m \text{ km}}{M_\odot R} + 90 \left(\frac{m \text{ km}}{M_\odot R} \right)^4 \right]. \quad (\text{A9})$$

The above equation is found as an empirical relation by fitting to a sample of the equation of state [52]. In this work we consider two equations of state: AP4 and PAL1. While these two models do not cover the entire range of possible equations of state that survive astrophysical constraints (see Ref. [53] for a recent review), they are chosen for illustrative purposes. For a typical NS mass of $1.4M_\odot$, the NS radius is 11 km and 14 km for AP4 and PAL1 respectively.

Assuming K remains a constant throughout the binary's lifetime, it is straightforward to show that the spin angular frequency at coalescence is:

$$\omega_f = \frac{\omega_i}{\sqrt{1 + 2T_c |\dot{\omega}_i| / \omega_i}}, \quad (\text{A10})$$

where ω_i and $\dot{\omega}_i$ are the initial values of angular spin frequency and its time derivative respectively.

It is possible that the NS magnetic field decays exponentially over time [20, 54–57]

$$B(t) = B_0 e^{-t/\tau_B}, \quad (\text{A11})$$

where τ_B is the magnetic field decay timescale. Under this decaying-B field model, the final spin frequency is

$$\omega_f = \frac{\omega_i}{\sqrt{1 + \tau_B [\exp(-2T_c/\tau_B) - 1] \dot{\omega}_i / \omega_i}}. \quad (\text{A12})$$

Appendix B: Construction of fiducial models

In this section we describe the construction of our models for the distribution of BNS parameters at birth $\pi(\vec{\lambda}_0)$. The models are fully motivated by pulsar observations of currently known Galactic BNS systems. These observations are summarized in Table III, including current and final (i.e., when binary merges) spin periods, the corresponding dimensionless spin magnitudes, binary orbital period and eccentricity, coalescence time, characteristic age and surface magnetic field strength, masses of the pulsar and its companion.

In our fiducial model, each binary consists of a recycled NS and a “normal” NS. Here “normal” means that it is born with a period of $\gtrsim 10$ ms but quickly spins down to $\mathcal{O}(1)$ seconds period over ~ 10 Myr [75]. PSR J1906+0746 is considered to be normal (similar to an isolated pulsar) because it is a young (~ 100 kyr) pulsar with much higher spin-down rate 2×10^{-14} [76]. As such, we consider its companion as a recycled NS. Table IV summarizes information about our fiducial BNS population models. We describe the details below.

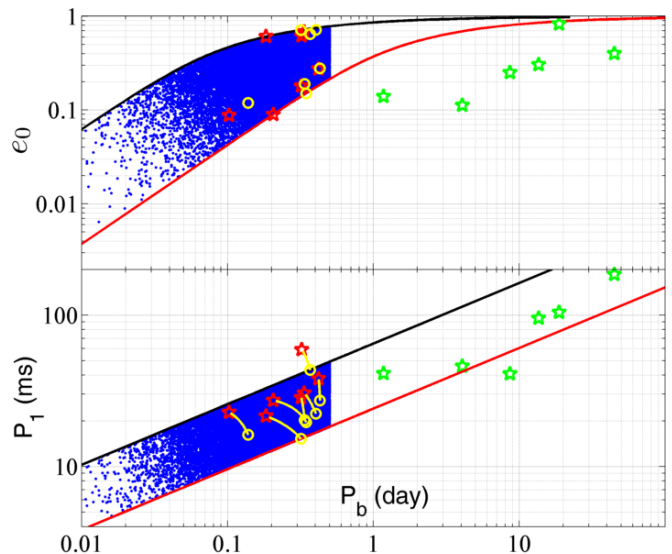


FIG. 7. A simulated BNS population (blue dots), along with known Galactic binary pulsar systems (open stars). Red (green) stars are for systems that will (will not) merge within a Hubble time. Yellow circles indicate the system states at the birth of the second NS. Yellow curves in the bottom panel indicate the evolutionary tracks back in time by half of the characteristic age of the recycled pulsar. Red and black lines set the restricted region for our fiducial population model.

We first derive a model for NS mass distribution from 10 BNS systems that have precise component mass measurements. To represent the full range of mass ratio between the recycled NS and its companion, we fit separately a two-Gaussian model to 10 measurements. For the recycled NS, the main peak of the mass distribution is centered around $1.35 M_\odot$ and the second around $1.57 M_\odot$, with weight of approximately 80% and 20% respectively. While the major Gaussian component is consistent with previous estimates (e.g., [77, 78]), the minor peak is intuitively contributed by the two high mass systems PSR J0453+1559 and PSR J1913+1102. For the non-recycled NS, the major Gaussian component is centered around $1.24 M_\odot$ and the second around $1.37 M_\odot$, with weight of about 60% and 40% respectively.

We assume P_b is uniformly distributed in the range of (0.01, 0.5) days. This corresponds to the range of measured orbital periods of Galactic BNS systems that will merge within a Hubble time, except that we extend to $P_b \lesssim 0.1$ day. Current searches for radio pulsars in relativistic binaries are limited to orbital periods longer than a few hours. The exact value of the lower cut for P_b has no significant impact as the population is dominated by systems in wider orbits. We assume that the initial spin period (P_1) of the recycled NS and the orbital eccentricity (e_0) are also uniformly distributed but are correlated with P_b as described below.

Figs. 7 and 8 provide an intuitive picture about the initial distributions of BNS parameters in our fiducial model. Blue dots mark the positions of synthetic BNS

Pulsar Name	P (ms)	P_f (ms)	χ_i	χ_f	P_b (days)	e_0	T_c (Gyr)	Age (Gyr)	B (10^9 G)	m_p (M_\odot)	m_c (M_\odot)	Ref.
systems will merge within a Hubble time												
J1757–1854	21.50	24.29	0.023	0.020	0.184	0.606	0.076	0.13	1.3	1.338	1.395	[58]
J0737–3039A	22.70	27.17	0.022	0.018	0.102	0.088	0.086	0.204	1.1	1.338	1.249	[59]
J0737–3039B	2773	4596	0	0	0.102	0.088	0.086	0.049	260	1.249	1.338	[59]
J1913+1102 ^a	27.29	29.59	0.016	0.015	0.206	0.090	0.473	2.685	0.4	1.61	1.27	[60]
J1756–2251	28.46	61.95	0.017	0.008	0.320	0.181	1.656	0.043	0.9	1.341	1.230	[61]
B2127+11C	30.53	54.90	0.016	0.009	0.335	0.681	0.217	0.097	2.2	1.358	1.354	[62]
B1534+12	37.90	131.5	0.013	0.004	0.421	0.274	2.734	0.248	1.7	1.333	1.346	[63]
B1913+16	59.03	114.6	0.008	0.004	0.323	0.617	0.301	0.109	4.1	1.440	1.389	[64]
J1906+0746	144.1	7636	0.004	0	0.166	0.085	0.308	0.0001	289	1.291	1.322	[65]
systems will not merge within a Hubble time												
J1807–2500B	4.19	150.8	0.117	0.003	9.957	0.747	1044	0.81	0.1	1.366	1.206	[66]
J1518+4904	40.93	792.4	0.013	0	8.634	0.249	8914	2.39	0.2	$M_{\text{tot}} = 2.72M_\odot$		[67]
J1829+2456	41.01	95.96	0.013	0.005	1.176	0.139	55.42	1.24	0.2	$M_{\text{tot}} = 2.59M_\odot$		[68]
J0453+1559	45.78	885.1	0.010	0	4.072	0.113	1453	3.90	0.6	1.559	1.174	[69]
J1753–2240	95.14	-	0.005	0	13.64	0.304	3×10^4	1.55	1.7	-	-	[70]
J1811–1736	104.2	-	0.004	0	18.78	0.828	1862	1.83	1.9	$M_{\text{tot}} = 2.57M_\odot$		[71]
J1930–1852	185.5	-	0.003	0	45.06	0.399	5×10^5	0.16	9.7	$M_{\text{tot}} = 2.59M_\odot$		[72]

^a Component mass measurements were reported by R. Ferdman at the IAU Symposia 337: “Pulsar Astrophysics - The Next 50 Years” and can be found at <http://pulsarastronomy.net/iaus337/post-meeting/presentations/>

TABLE III. Spin periods and dimensionless spin magnitudes at the present (P and χ_i) and upon coalescence (P_f and χ_f) for pulsars in known Galactic BNS systems. $\chi < 10^{-3}$ is listed as 0 and $P_f > 10$ s is considered as irrelevant in this table. We assume that the spin evolution is determined by magnetic dipole braking, the magnetic field does not decay and use the AP4 equation of state. Also included are binary orbital period (P_b), orbital eccentricity (e_0), coalescence time T_c , characteristic age ($P/2\dot{P}$ where \dot{P} is the observed spin period derivative), magnetic field strength (B), the mass of the pulsar (m_p) and its companion (m_c). The total mass (M_{tot}) is listed when no definitive component mass measurements. Note that 1) PSR J1906+0746 is considered as a “normal” NS and its companion’s mass is included in the fit for mass distribution of the recycled NS; and 2) PSR1807–2500B is not included in the P - P_b correlation used to build our empirical BNS population model.

Parameter	min	max	distribution	note/ correlation
P_1 (ms)	3.8	49	Uniform	Eq. (B1)
P_b (day)	0.01	0.5	Uniform	Eqs. (A5-A6)
e_0	0.004	0.78	Uniform	
$\log(B_1/\text{G})$	8.0	10	$N(9.1, 0.22)$	AP4
$\log(B_2/\text{G})$	8.0	10	$N(8.9, 0.22)$	PAL1
P_2 (ms)	10	900	$N(300, 150)$	[73, 74]
$\log(B_2/\text{G})$	10.5	15	$N(12.65, 0.55)$	[73, 74]
m_1 (M_\odot)	1.1	2.0	$0.77 \times N(1.35, 0.06)$ $+0.23 \times N(1.57, 0.08)$	NS radius
m_2 (M_\odot)	1.0	1.6	$0.63 \times N(1.24, 0.06)$ $+0.37 \times N(1.37, 0.05)$	

TABLE IV. The minimum and maximum values and the distributions of NS parameters used to build our fiducial BNS population models described in Section II. P_1 (B_1) and P_2 (B_2) are the initial spin period (magnetic field strength) for the recycled NS (first formed) and its companion respectively. m_1 and m_2 is mass for the recycled NS and the secondly born NS respectively. We use a two-Gaussian model for the NS mass distribution. Note that different mean values are needed for B_1 for two different equations of state.

systems, whereas open stars represent known Galactic systems. Red (green) stars are for binaries that will (will not) merge within a Hubble time. Yellow open circles are obtained by evolving red stars back in time, indicating the initial conditions when the second NS was born.

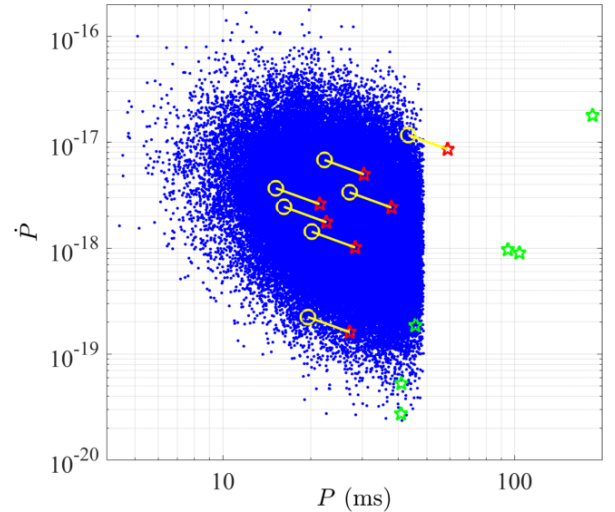


FIG. 8. The same as Fig. 7 but for the $P - \dot{P}$ parameter space of the recycled NS.

In the lower panel of Fig. 7, open stars indicate positions of recycled pulsars in BNS systems in the orbital period – spin period diagram. As one can see, there exists a linear correlation for $\log P_b - \log P_1$

$$P_1 = P_{\text{ref}}(P_b/P_{b,\text{ref}})^\gamma. \quad (\text{B1})$$

Here we consider $\gamma = 0.4$ (the slope for black and red

straight lines) as found by a fit to 11 Galactic BNS systems studied in [9]. Such a linear correlation is further confirmed by the 13 BNS systems considered in this work. P_{ref} and $P_{b,\text{ref}}$ are reference values used to determine the boundary region in the parameter space.

In order to obtain the initial values of P_b , P_1 , \dot{P} and e_0 for 7 Galactic BNS systems at the birth of the second NS, we evolve these systems back in time assuming magnetic dipole braking and GW-driven orbital decay. The time is set as half of the characteristic age. Although this is somewhat arbitrary, it should be noted that the spin period approaches zero when evolving the pulsar back by the full amount of its characteristic age. The evolution is shown as yellow tracks in the bottom panel of Fig. 7 and Fig. 8. The upper bound (black line) in the P_b - P_1 plane is set by PSR J1756–2251 with initial orbital period of 0.37 day and spin period of 43 ms. The lower bound (red line) is set by PSR J1757–1854 with initial orbital period of 0.32 day and spin period of 15 ms. The black and red lines, together with the cut-off in orbital period, determine the maximum and minimum values for P_1 to be 49 and 4 ms respectively.

In the top panel of Fig. 7, we show the restricted region in the P_b - e_0 plane for our fiducial BNS population model. In the GW-driven regime, P_b and e_0 co-evolve following equations (A5-A6). This is indicated by red and black curves, which cross J1913+1102 and J1757–1854 respectively. Such a choice excludes binary systems with either very short birth orbital periods and high eccentricities (top-left corner) or long periods and low eccentricities (bottom-right corner), as both are shown to be unlikely based on pulsar observations. Red and black curves, together with the cut-off in P_b , lead to a range of e_0 between 0.004 and 0.8.

We make use of NS mass-radius relation described by the AP4 and PAL1 equation of state. The magnetic field strength of the recycled NS at the time of the birth of its companion is assumed to follow a log-Normal distribution with a mean value $\mu_{\log,B} = 9.1$ (8.9) and a standard

deviation $\sigma_{\log,B} = 0.22$ for the AP4 (PAL1) equation of state. Such a distribution is found to be able to cover the scatter in the P - \dot{P} diagram for recycled pulsars at the birth of second NS considered in this work, as demonstrated in Fig. 8. Because PAL1 allows relatively large NS radii, the required magnetic field strength to produce the same spin-down rate is lower; see Eq. (A8). This illustrates the covariance between the equation of state and the magnetic field in probing NS spin evolution. Future GW measurements of NS tidal effects and possibly post-merger signatures are likely to place tight constraints on the equation of state. This will enable better understanding on NS magnetic field evolution through spin measurements.

For the second-born NS, we assume that i) the initial spin period follows a Gaussian distribution with a mean of 300 ms and a standard deviation of 150 ms [73, 74]; and ii) the initial magnetic field strength follows a log-Normal distribution with a mean $\mu_{\log,B} = 12.65$ and a standard deviation $\sigma_{\log,B} = 0.55$ [73]. Note that our results are insensitive to details of these two distributions as in our fiducial model the second NS makes no contribution to χ_{eff} unless the magnetic field decay timescale is much shorter than binary coalescence time.

Finally, we briefly comment on directions to improve the fiducial models presented here. Our primary goal in developing these fiducial models was to cover parameter ranges informed by pulsar observations. Some prescriptions are therefore ad-hoc. We assume the magnetic field strength remains a constant when evolving the recycled pulsars back in time to obtain the initial distributions of spin periods and period derivatives. However, we allow magnetic field to decay when evolving $\pi(\vec{\lambda}_0)$ forward in time to obtain at-merger distribution $\pi(\vec{\lambda}_m)$. While this inconsistency does not significantly impact our results, future models should include a self-consistent treatment of magnetic field decay.

-
- [1] J. Aasi *et al.*, *Classical and Quantum Gravity* **32**, 074001 (2015).
 - [2] F. Acernese *et al.*, *Classical and Quantum Gravity* **32**, 024001 (2015), arXiv:1408.3978 [gr-qc].
 - [3] B. P. Abbott *et al.* (LIGO Scientific Collaboration and Virgo Collaboration), *Phys. Rev. Lett.* **119**, 161101 (2017).
 - [4] B. P. Abbott *et al.*, *The Astrophysical Journal Letters* **848**, L12 (2017).
 - [5] I. Andreoni *et al.*, *ArXiv e-prints* (2017), arXiv:1710.05846 [astro-ph.HE].
 - [6] J. Abadie *et al.*, *Classical and Quantum Gravity* **27**, 173001 (2010), arXiv:1003.2480 [astro-ph.HE].
 - [7] R. A. Hulse and J. H. Taylor, *Astrophys. J.* **191**, L59 (1974).
 - [8] R. A. Hulse and J. H. Taylor, *Astrophys. J.* **195**, L51 (1975).
 - [9] T. M. Tauris *et al.*, *Astrophys. J.* **846**, 170 (2017), arXiv:1706.09438 [astro-ph.HE].
 - [10] M. Burgay *et al.*, *Nature (London)* **426**, 531 (2003), astro-ph/0312071.
 - [11] A. G. Lyne *et al.*, *Science* **303**, 1153 (2004), astro-ph/0401086.
 - [12] A. Tutukov and L. Yungelson, *Nauchnye Informatsii* **27**, 70 (1973).
 - [13] B. P. Flannery and E. P. J. van den Heuvel, *A&A* **39**, 61 (1975).
 - [14] L. L. Smarr and R. Blandford, *Astrophys. J.* **207**, 574 (1976).
 - [15] V. Kalogera, K. Belczynski, C. Kim, R. O’Shaughnessy, and B. Willems, *Physics Reports* **442**, 75 (2007).
 - [16] K. A. Postnov and L. R. Yungelson, *Living Reviews in Relativity* **17**, 3 (2014), arXiv:1403.4754 [astro-ph.HE].
 - [17] P. Goldreich and W. H. Julian, *Astrophys. J.* **157**, 869

- (1969).
- [18] I. Contopoulos, D. Kazanas, and C. Fendt, *Astrophys. J.* **511**, 351 (1999), astro-ph/9903049.
- [19] A. Spitkovsky, *Astrophys. J.* **648**, L51 (2006), astro-ph/0603147.
- [20] A. Bransgrove, Y. Levin, and A. Beloborodov, *ArXiv e-prints* (2017), arXiv:1709.09167 [astro-ph.HE].
- [21] P. Ajith, M. Hannam, S. Husa, *et al.*, *Phys. Rev. Lett.* **106**, 241101 (2011), arXiv:0909.2867 [gr-qc].
- [22] C. Cutler, T. A. Apostolatos, L. Bildsten, *et al.*, *Phys. Rev. Lett.* **70**, 2984 (1993), astro-ph/9208005.
- [23] B. P. Abbott *et al.*, *Astrophys. J.* **832**, L21 (2016), arXiv:1607.07456 [astro-ph.HE].
- [24] T. Dietrich, N. Moldenhauer, N. K. Johnson-McDaniel, S. Bernuzzi, C. M. Markakis, B. Brügmann, and W. Tichy, *Phys. Rev. D* **92**, 124007 (2015), arXiv:1507.07100 [gr-qc].
- [25] D. A. Brown, I. Harry, A. Lundgren, and A. H. Nitz, *Phys. Rev. D* **86**, 084017 (2012), arXiv:1207.6406 [gr-qc].
- [26] S. Vitale, R. Lynch, R. Sturani, and P. Graff, *Classical and Quantum Gravity* **34**, 03LT01 (2017), arXiv:1503.04307 [gr-qc].
- [27] S. Stevenson, C. P. L. Berry, and I. Mandel, *Mon. Not. R. Astron. Soc.* **471**, 2801 (2017), arXiv:1703.06873 [astro-ph.HE].
- [28] C. Talbot and E. Thrane, *Phys. Rev. D* **96**, 023012 (2017), arXiv:1704.08370 [astro-ph.HE].
- [29] W. M. Farr, S. Stevenson, M. C. Miller, I. Mandel, B. Farr, and A. Vecchio, *Nature (London)* **548**, 426 (2017), arXiv:1706.01385 [astro-ph.HE].
- [30] While it is incorrect that the spin-down is due to magnetic dipole radiation, it is the dipole that plays the key role and the dipole spin-down formula is correct to order unity.
- [31] R. D. Ferdman *et al.*, *Astrophys. J.* **767**, 85 (2013), arXiv:1302.2914 [astro-ph.SR].
- [32] J. M. Lattimer and M. Prakash, *Astrophys. J.* **550**, 426 (2001), astro-ph/0002232.
- [33] This is used just as an example of the field evolution. Bransgrove *et al.* did not consider recycled pulsars in detail in their scenario (much colder crust with the field affected by accretion).
- [34] S. Osłowski, T. Bulik, D. Gondek-Rosińska, and K. Belczyński, *Mon. Not. R. Astron. Soc.* **413**, 461 (2011), arXiv:0903.3538 [astro-ph.GA].
- [35] We use the standard zero detuning high power sensitivity curve, which is publicly available at <https://dcc.ligo.org/LIGO-T0900288/public>. For the simplicity of calculations and computational cost with LALINFERENCE runs, we do not consider the other advanced detectors. This only makes our conclusions more conservative.
- [36] J. Veitch *et al.*, *Phys. Rev. D* **91**, 042003 (2015), arXiv:1409.7215 [gr-qc].
- [37] M. Hannam, P. Schmidt, A. Bohé, L. Haegel, S. Husa, F. Ohme, G. Pratten, and M. Pürrer, *Physical Review Letters* **113**, 151101 (2014), arXiv:1308.3271 [gr-qc].
- [38] R. Smith, S. E. Field, K. Blackburn, C.-J. Haster, M. Pürrer, V. Raymond, and P. Schmidt, *Phys. Rev. D* **94**, 044031 (2016), arXiv:1604.08253 [gr-qc].
- [39] T. Dietrich, S. Bernuzzi, and W. Tichy, *ArXiv e-prints* (2017), arXiv:1706.02969 [gr-qc].
- [40] C. Cutler and É. E. Flanagan, *Phys. Rev. D* **49**, 2658 (1994), gr-qc/9402014.
- [41] J. Abadie *et al.*, *Phys. Rev. D* **85**, 082002 (2012), arXiv:1111.7314 [gr-qc].
- [42] B. F. Schutz, *Classical and Quantum Gravity* **28**, 125023 (2011), arXiv:1102.5421 [astro-ph.IM].
- [43] In this work we treat the recycled NS instead of the more massive one as the primary star, so it is possible that $q > 1$. In this case, which corresponds to $\approx 20\%$ of all BNSs given the fiducial mass distributions derived in Section B, we use $1/q$ for the range quoted here.
- [44] D. J. C. MacKay, *Information Theory, Inference & Learning Algorithms* (Cambridge University Press, New York, NY, USA, 2002).
- [45] K. Somiya, *Classical and Quantum Gravity* **29**, 124007 (2012), arXiv:1111.7185 [gr-qc].
- [46] C. S. Unnikrishnan, *International Journal of Modern Physics D* **22**, 1341010 (2013), arXiv:1510.06059 [physics.ins-det].
- [47] B. D. Lackey and L. Wade, *Phys. Rev. D* **91**, 043002 (2015), arXiv:1410.8866 [gr-qc].
- [48] K. S. Thorne, in *Hawking S., Israel W., eds, Three Hundred Years of Gravitation* (Cambridge Uni. Press, Cambridge, 1987) p. 330.
- [49] P. C. Peters and J. Mathews, *Physical Review* **131**, 435 (1963).
- [50] P. C. Peters, *Physical Review* **136**, 1224 (1964).
- [51] J. P. Ostriker and J. E. Gunn, *Astrophys. J.* **157**, 1395 (1969).
- [52] J. M. Lattimer and B. F. Schutz, *Astrophys. J.* **629**, 979 (2005), astro-ph/0411470.
- [53] J. M. Lattimer, *Annual Review of Nuclear and Particle Science* **62**, 485 (2012), arXiv:1305.3510 [nucl-th].
- [54] R. W. Romani, *Nature (London)* **347**, 741 (1990).
- [55] U. Geppert and V. Urpin, *Mon. Not. R. Astron. Soc.* **271** (1994), 10.1093/mnras/271.2.490.
- [56] S. Konar and D. Bhattacharya, *Mon. Not. R. Astron. Soc.* **284**, 311 (1997).
- [57] A. Cumming, P. Arras, and E. Zweibel, *Astrophys. J.* **609**, 999 (2004), astro-ph/0402392.
- [58] A. D. Cameron *et al.*, *ArXiv e-prints* (2017), arXiv:1711.07697 [astro-ph.HE].
- [59] M. Kramer *et al.*, *Science* **314**, 97 (2006), astro-ph/0609417.
- [60] P. Lazarus *et al.*, *Astrophys. J.* **831**, 150 (2016), arXiv:1608.08211 [astro-ph.HE].
- [61] R. D. Ferdman *et al.*, *Mon. Not. R. Astron. Soc.* **443**, 2183 (2014), arXiv:1406.5507 [astro-ph.SR].
- [62] B. A. Jacoby, P. B. Cameron, F. A. Jenet, S. B. Anderson, R. N. Murty, and S. R. Kulkarni, *Astrophys. J.* **644**, L113 (2006), astro-ph/0605375.
- [63] E. Fonseca, I. H. Stairs, and S. E. Thorsett, *Astrophys. J.* **787**, 82 (2014), arXiv:1402.4836 [astro-ph.HE].
- [64] J. M. Weisberg, D. J. Nice, and J. H. Taylor, *Astrophys. J.* **722**, 1030 (2010), arXiv:1011.0718 [astro-ph.GA].
- [65] J. van Leeuwen *et al.*, *Astrophys. J.* **798**, 118 (2015), arXiv:1411.1518 [astro-ph.SR].
- [66] R. S. Lynch, P. C. C. Freire, S. M. Ransom, and B. A. Jacoby, *Astrophys. J.* **745**, 109 (2012), arXiv:1112.2612 [astro-ph.HE].
- [67] G. H. Janssen, B. W. Stappers, M. Kramer, D. J. Nice, A. Jessner, I. Cognard, and M. B. Purver, *A&A* **490**, 753 (2008), arXiv:0808.2292.
- [68] D. J. Champion, D. R. Lorimer, M. A. McLaughlin, K. M. Xilouris, Z. Arzoumanian, P. C. C. Freire, A. N.

- Lommen, J. M. Cordes, and F. Camilo, *Mon. Not. R. Astron. Soc.* **363**, 929 (2005), astro-ph/0508320.
- [69] J. S. Deneva, K. Stovall, M. A. McLaughlin, S. D. Bates, P. C. C. Freire, J. G. Martinez, F. Jenet, and M. Bagchi, *Astrophys. J.* **775**, 51 (2013), arXiv:1307.8142 [astro-ph.SR].
- [70] M. J. Keith, M. Kramer, A. G. Lyne, R. P. Eatough, I. H. Stairs, A. Possenti, F. Camilo, and R. N. Manchester, *Mon. Not. R. Astron. Soc.* **393**, 623 (2009), arXiv:0811.2027.
- [71] A. Corongiu, M. Kramer, B. W. Stappers, A. G. Lyne, A. Jessner, A. Possenti, N. D'Amico, and O. Löhmer, *A&A* **462**, 703 (2007), astro-ph/0611436.
- [72] J. K. Swiggum *et al.*, *Astrophys. J.* **805**, 156 (2015), arXiv:1503.06276 [astro-ph.HE].
- [73] C.-A. Faucher-Giguère and V. M. Kaspi, *Astrophys. J.* **643**, 332 (2006), astro-ph/0512585.
- [74] J. P. Ridley and D. R. Lorimer, *Mon. Not. R. Astron. Soc.* **404**, 1081 (2010), arXiv:1001.2483.
- [75] D. R. Lorimer and M. Kramer, *Handbook of pulsar astronomy*, Vol. 4 (Cambridge University Press, 2005).
- [76] D. R. Lorimer *et al.*, *Astrophys. J.* **640**, 428 (2006), astro-ph/0511523.
- [77] F. Özel, D. Psaltis, R. Narayan, and A. Santos Villarreal, *Astrophys. J.* **757**, 55 (2012), arXiv:1201.1006 [astro-ph.HE].
- [78] B. Kiziltan, A. Kottas, M. De Yoreo, and S. E. Thorsett, *Astrophys. J.* **778**, 66 (2013), arXiv:1011.4291.